Pergamon

Geochimica et Cosmochimica Acta, Vol. 67, No. 8, pp. 1451–1461, 2003

0016-7037/03 $30.00 + .00

doi:10.1016/S0016-7037(02)01293-0

Chlorite dissolution in the acid pH-range: A combined microscopic and macroscopic approach

FELIX BRANDT,[1,*] DIRK BOSBACH,[1] EVELYN KRAWCZYK-BÄRSCH,[2] THURO ARNOLD,[2] and GERT BERNHARD[2]

[1]Institut für Nukleare Entsorgung (INE), Forschungszentrum Karlsruhe, Hermann-von-Helmholtz-Platz 1, 76344 Eggenstein-Leopoldshafen, Germany

[2]Institut für Radiochemie, Forschungszentrum Rossendorf, Bautzner Landstraβe 128, 01328 Dresden, Germany

(*Received March* 22, 2002; *accepted in revised form October* 15, 2002)

Abstract—The dissolution of chlorite with intermediate Fe-content was studied macroscopically via mixed flow experiments as well as microscopically via atomic force microscopy (AFM). BET surface area normalized steady state dissolution rates at 25 °C for pH 2 to 5 vary between 10^{-12} and 10^{-13} mol/m^2·s. The order of the dissolution reaction with respect to protons was calculated to be about 0.29. For pH 2 to 4, chlorite was found to dissolve non-stoichiometrically, with a preferred release of the octahedrally coordinated cations. The additional release of octahedrally coordinated cations may be due to the transformation of chlorite to interstratified chlorite/vermiculite from the grain edges inward.

In-situ atomic force microscopy performed on the basal surfaces of a chlorite sample, which has been preconditioned at pH 2 for several months, indicated a defect controlled dissolution mechanism. Molecular steps with height differences which correspond to the different subunits of chlorite, e.g. TOT sheet and brucite like layer, originated at surface defects such or compositional inhomogenities or cracks, which may be due to the deformation history of the chlorite sample. In contrast to other sheet silicates, at pH 2 nanoscale etch pits occur on the chlorite basal surfaces within flat terraces terminated by a TOT-sheet as well as within the brucite like layer. The chlorite basal surface dissolves layer by layer, because most of the surface defects are only expressed through single TOT or brucite-like layers. The defect controlled dissolution mechanism favours dissolution of molecular steps on the basal surfaces compared to dissolution of the grain edges. At pH 2 the dissolution of the chlorite basal surface is dominated by the retreat of 14 Å steps, representing one chlorite unit cell.

The macroscopic and microscopic chlorite dissolution rates can be linked via the reactive surface area as identified by AFM. The reactive surface area with respect to dissolution consists of only 0.2% of the BET-surface area. A dissolution rate of 2.5×10^{-9} mol/m^{2}s was calculated from macroscopic and microscopic dissolution experiments at pH 2, when normalized to the reactive surface area. *Copyright © 2003 Elsevier Science Ltd*

1. INTRODUCTION

In nature, primary chlorite, which has been formed under metamorphic conditions, is unstable under acidic weathering conditions (Barnhisel and Bertsch, 1989). Due to its structural complexity and chemical variability, the dissolution of chlorite involves several mechanisms (Coffman and Fanning, 1975; Herbillon and Makumbi, 1975; Adams, 1976; Bain, 1977; Adams and Kassim, 1983). Primary chlorites can transform into regularly and irregularly interstratified vermiculite/smectite as a consequence of preferential leaching of certain cations from the chlorite structure (Banfield and Murakami, 1998). A further consequence of the preferential cation release is the potential precipitation of secondary phases on the primary or altered chlorite phases. Because of their high specific surface area and their high affinity for many contaminants (e.g., heavy metals, radionuclides), hydrous ferrous oxide (HFO) phases are important secondary precipitates which form coatings on mineral substrates (Hochella et al., 1999; Krawczyk-Bärsch et al., 2001). The altered chlorite and the secondary HFO phases control the chemical behavior of phyllite rocks with respect to many geochemical processes in the environment including the transport of contaminants (e.g., heavy metals, radionuclides) through such a system (Arnold et al., 2001).

To unravel the mechanism for the dissolution of chlorite, a detailed knowledge of the stoichiometry and the dissolution rate as well as the reactive surface area involved with the dissolution reaction is needed. Mixed-flow reactor experiments can be used as a tool to quantify surface reaction controlled dissolution. For chlorite, macroscopic dissolution rates in the acid pH range obtained from such experiments are limited to a few studies only (Ross, 1969; May et al., 1995; Rochelle et al., 1996; Salmon and Malmström, 2001; Lowson et al., 2002). According to these studies, the BET-surface area normalized, steady state dissolution rate obtained far from equilibrium under acidic conditions varies between 10^{-11} mol/m^{2}s for pH 3 and 10^{-13} mol/m^{2}s for the neutral pH range (May et al., 1995; Lowson et al., 2002). In some studies, Chlorite dissolution in the acid pH range is reported to be incongruent, i.e., the octahedrally coordinated cations Mg, Fe, Al are released at a higher rate than Si (May et al., 1995).

Apart from the element release rate, which can directly be determined from macroscopic dissolution experiments, the reactive surface area, to which these rates should be normalized, is a critical parameter with regard to the dissolution reaction. Macroscopic dissolution studies in general assume that the BET surface area is identical with the reactive surface area.

* Author to whom correspondence should be addressed (felix@ine.fzk.de).

Table 1. Chemical composition of the chlorite samples.

	Chlorite CCa-2 Flagstaff Hill, California	Chlorite MaIn Mangalapur, India
SiO_2	26,15	26,83
Al_2O_3	21,13	21,64
Fe_2O_3	5,93	6,07
FeO	17,20	13,3
MgO	17,73	20,67
Loss on Ignition (LOI)	9.23	9,95
Σ	97,37	98,46

Determined by EMP except for FeO, determined by titration.

Table 2. Distribution of cations in the chlorite structure based on the model presented in the text.

Number of atoms in the TOT-layer	$Si^{[4]}$	$Al^{[4]}$	$Mg^{[6]}$	$Fe(II)^{[6]}$	$Fe(III)^{[6]}$
CCa-2	5.33	2.67	3.38	1.68	0.94
MaIn	5.33	2.67	3.44	1.67	0.89
Number of atoms in the brucite layer	**$Al^{[6]}$**	**$Mg^{[6]}$**	**$Fe(II)^{[6]}$**	**$Fe(III)^{[6]}$**	
CCa-2	2.48	2.16	1.34	–	
MaIn	2.47	2.89	0.64	–	

Often a linear relationship between the BET surface area and the dissolution rate is assumed and that this relationship is independent of pH and temperature (Ganor et al., 1995). However, there are numerous examples where there is no linear relationship between the BET surface area and the dissolution rate, indicating that the reactive surface area is not equivalent to the BET surface area. Various recent studies have demonstrated that the dissolution of sheet silicates is limited to small fractions of the overall surface (Rufe and Hochella Jr., 1999; Bosbach et al., 2000; Bickmore et al., 2001). Here, we have used the same chlorite samples in a combination of experiments on the microscopic and the microscopic scale in order identify the reactive surface area and the mechanisms controlling the kinetics of cation release during chlorite dissolution in the acid pH-range.

2. MATERIAL AND METHODS

2.1. Sample Description

Chlorite schists from (1) Flagstaff Hill, California, the source clay standard **CCa-2** from the Clay Minerals Society, and (2) from Mangalapur, India **(MaIn)**, which was obtained from the mineral collection of the Institut für Mineralogie, Universität Münster (Germany), were used to prepare chlorite suspensions for this study.

2.1.1. Sample composition

Both samples were analysed for impurities intergrown with chlorite using X-ray diffraction (XRD), electron microprobe (EMP) and scanning electron microscopy (SEM). Within the detection limit of XRD (~5%) both samples are pure chlorite. EMP revealed small amounts of impurities (<1%) of illmenite and titanite (only CCa-2). The average chlorite compositions (Table 1) were determined from electron microprobe analysis (EMP) and titration of each completely dissolved chlorite sample for Fe^{2+}/Fe^{3+} (method described in detail in Herrmann, 1975) as:

$$\text{CCa-2 } (Mg_{5.54}Fe^{2+}_{3.02}Fe^{3+}_{0.94}Al_{2.48})[Si_{5.33}Al_{2.66}O_{20}](OH)_{16} \quad (1)$$

$$\text{MaIn } (Mg_{6.33}Fe^{2+}_{2.27}Fe^{3+}_{0.93}Al_{2.48})[Si_{5.33}Al_{2.66}O_{20}](OH)_{16} \quad (2)$$

In general, structural refinements based on XRD and Mössbauer spectroscopy indicate a systematic ordering scheme for the distribution of cations in the chlorite structure with its TOT and brucite-like layer (Joswig et al., 1980; Rule and Bailey, 1987; Lougear et al., 2000). According to this ordering scheme, Si exclusively occupies tetrahedral sites in the TOT sheet. The tetrahedral sites not occupied by Si are filled up with Al. Further Al is supposed to be octahedrally coordinated and placed in the brucite-like layer (Steinfink, 1958a; Steinfink, 1958b; Steinfink, 1961; Brindley and Brown, 1984). The symmetry of the Fe distribution between the TOT and brucite-like layers (Table 2) can be roughly estimated from the intensities of the (002), (003), (004) and (005) XRD basal reflections (Brindley and Brown, 1984; Moore and Reynolds, 1997). Mössbauer and molecular orbital studies indicate that Fe^{2+} is most likely located in the octahedrally coordinated M1 and M2 positions of the TOT sheet (Lougear et al., 2000). Mg occupies those octahedral sites left over after Fe and Al are distributed over the structure.

According to this ordering scheme, one major crystal chemical difference between the two chlorite samples used in this study is that in sample CCa-2 ~33% of the total Fe is located in the brucite layer, but only 20% of the total Fe in the MaIn. The TOT sheets of the two samples are quite similar in their composition (Table 2).

2.1.2. Sample preparation

For the mixed flow reactor (MFR) experiments, chlorite powders were prepared from chlorite schists. First the chlorite schists were mechanically broken to pieces in the cm-range. These pieces were subjected to heating-cooling cycles (−200°C to room temperature) using liquid nitrogen. Compared to breaking down the sample with a ball mill, this procedure should minimize mechanical and chemical alteration of the sample due to the preparation. Mechanical and chemical alteration could potentially affect the dissolution behaviour, e.g., the time until steady state is reached. The size fraction 63 to 200 μm was obtained by sieving and used for the macroscopic experiments. For the microscopic experiments the size fraction 63 to 10 μm was used because it was less difficult to prepare for the AFM measurements. After these preparation steps, no impurities were found in the final chlorite samples with X-ray diffraction or electron microscopy. Therefore, illmenite and titanite are enriched in a size fraction which is not used for the experiments presented here.

2.1.3. The specific surface area

Surface reaction controlled mineral dissolution rates are a function of the number of the reactive sites at the mineral/solution interface. Within the framework of transition state theory, the number of the reactive sites depends on the density of activated complex sites on the mineral surfaces (a function of pH) and the amount of surface area exposed to solution that contains theses sites (Nagy, 1995). Therefore, the mineral surface area represents an important parameter that is used to extrapolate from the atomic surface to the field scale (White and Brantley, 1995).

Various approaches have been used to determine the mineral surface area. In studies, where the dissolution of single crystals was examined, the geometric surface area (GSA) was determined from the lengths and widths of individual crystal surfaces using light microscopy (e.g., Turpault and Trotignon, 1994) or electron microscopy. For powders, the specific surface area is commonly determined by the BET gas adsorption method (Brunauer et al., 1938).

Commonly macroscopic dissolution studies implicitly assume that the dissolution rate is directly proportional to the BET surface area (May et al., 1995; Malmström et al., 1996; Malmström and Banwart, 1997; Cama et al., 1999; Metz and Ganor, 2001). However, there are numerous examples where no linear relationship between BET surface area and dissolution rate exists, indicating that the reactive surface area of some minerals is different from the total surface area as measured with the BET method (several examples reviewed in Brantley and

Table 3a. Chlorite steady state dissolution rates and experimental conditions for the MFR experiments conducted in this study. All experiments were performed at 25°C. The highlighted concentrations were used for the speciation calculations presented in table 3b.

Experiment No.	Chlorite sample	Element	pH (effluent)	Ionic strength	Steady state concentration [μmol/l]	Pump rate [ml/min]	Measured after [hours]	Steady state rate [10^{-12} mol/m^{2}s]
1	MaIn	Si	1.99	not adjusted	0.93	0.84 ± 0.008	70.25	3.00 ± 0.45
1	MaIn	Si	1.89	not adjusted	0.86	0.84 ± 0.008	380–480	2.70 ± 0.41
1	MaIn	Fe	1.89	not adjusted	0.90	0.84 ± 0.008	431–521	4.87 ± 0.73
1	MaIn	Mg	1.89	not adjusted	1.77	0.84 ± 0.008	431–521	5.36 ± 0.80
1	MaIn	Al	1.89	not adjusted	1.67	0.84 ± 0.008	431–521	5.60 ± 0.80
2	CCa-2	Si	2.10	not adjusted	0.78	0.73 ± 0.007	408–473	3.21 ± 0.35
2	CCa-2	Fe	2.10	not adjusted	0.91	0.73 ± 0.007	300–473	5.18 ± 0.78
2	CCa-2	Mg	2.10	not adjusted	1.42	0.73 ± 0.007	473	5.36 ± 0.80
2	CCa-2	Al	2.10	not adjusted	1.26	0.73 ± 0.007	473	5.60 ± 0.84
3	CCa-2	Si	1.95	0.1 mol/l $NaClO_4$	0.50	0.96 ± 0.01	90–200	2.75 ± 0.42
3	CCa-2	Fe	1.95	0.1 mol/l $NaClO_4$	0.64	0.96 ± 0.01	90–200	4.71 ± 0.71
4	CCa-2	Fe	1.96	0.1 mol/l $NaClO_4$	0.91	0.82 ± 0.01	112–140	5.32 ± 0.80
4	CCa-2	Mg	1.96	0.1 mol/l $NaClO_4$	1.26	0.82 ± 0.01	112–140	5.88 ± 0.88
4	CCa-2	Al	1.96	0.1 mol/l $NaClO_4$	1.26	0.82 ± 0.01	112–140	5.94 ± 0.89
5	CCa-2	Si	2.97	0.1 mol/l $NaClO_4$	0.45	0.79	168–220	2.00 ± 0.30
6	CCa-2	Si	3.11	0.1 mol/l $NaClO_4$	0.63	0.67	170–453	2.47 ± 0.37
5	CCa-2	Fe	2.97	0.1 mol/l $NaClO_4$	0.37	0.79	168–220	2.27 ± 0.34
6	CCa-2	Fe	3.11	0.1 mol/l $NaClO_4$	0.76	0.67	170–453	3.91 ± 0.59
7	CCa-2	Fe	3.01	0.1mol/l $NaClO_4$	0.59	0.80	146–190	3.77 ± 0.56
7	CCa-2	Mg	3.01	0.1mol/l $NaClO_4$	1.01	0.80	146–190	2.85 ± 0.43
7	CCa-2	Al	3.01	0.1mol/l $NaClO_4$	0.90	0.80	146–190	2.80 ± 0.30
8	CCa-2	Si	3.98	0.1mol/l $NaClO_4$	0.21	0.54	160–200	0.65 ± 0.10
8	CCa-2	Fe	3.98	0.1mol/l $NaClO_4$	0.33	0.54	160–200	1.33 ± 0.20
9	CCa-2	Mg	4.05	0.1mol/l $NaClO_4$	0.42	0.93	117–168	1.72 ± 0.26
9	CCa-2	Al	4.05	0.1mol/l $NaClO_4$	0.38	0.93	117–168	1.88 ± 0.28
10	CCa-2	Si	5.30	0.1mol/l $NaClO_4$	0.23	0.83	98–145	1.10 ± 0.17
10	CCa-2	Fe	5.30	0.1mol/l $NaClO_4$	0.20	0.83	73–145	1.30 ± 0.20
11	CCa-2	Fe	5.10	0.1mol/l $NaClO_4$	0.48	0.60	73	1.23 ± 0.25
11	CCa-2	Fe	5.10	0.1mol/l $NaClO_4$	0.36	0.91	170–194	1.45 ± 0.17
11	CCa-2	Mg	5.10	0.1mol/l $NaClO_4$	0.22–0.40	0.60–0.91	70–170	1.41 ± 0.16
11	CCa-2	Al	5.10	0.1mol/l $NaClO_4$	0.29–0.57	0.60–0.91	120–194	1.64 ± 0.25

Chen, 1995). Therefore we have determined not only the BET surface area, but also the GSA and the surface roughness of some of the chlorite samples used in this study. The surface roughness can be characterized quantitatively as the ratio BET surface area/geometric surface area (Helgeson et al., 1984).

The BET surface area was determined by a single point N_2-BET method as: CCa-2: 1.1 (± 0.1) m^2/g, MaIn: 1.6 (± 0.16) m^2/g. The geometric surface area (GSA) of the chlorite CCa-2 sample was determined from SEM observations of representative particles of the 63 to 200μm grain size fraction and varies between 0.06 m^2/g for large particles and 0.19 m^2/g for small particles. An average GSA was calculated to be 0.12 (± 0.05) m^2/g. This indicates a surface roughness of around 9 (± 3) for this sample. Microscopic examination of the fresh chlorite sample with the atomic force microscope indicates that the basal surfaces are very smooth except for cracks within the basal surfaces. However, these cracks amount to no more than ~1% of the total basal surface area. Therefore, the high surface roughness can very likely be attributed to the rugged edges of the chlorite crystals.

Recent studies have utilized AFM for the in-situ study of phyllosilicate dissolution to quantify the reactive surface area (Rufe and Hochella Jr., 1999; Bosbach et al., 2000; Bickmore et al., 2001). For small clay particles such as hectorite and nontronite and for micas such as phlogopite, the basal surfaces are nearly inert during dissolution, whereas the edge surfaces are highly reactive during dissolution. For the chlorite CCa-2 sample used in this study, SEM observations indicate that the edge surfaces make up ~20% of the GSA, whereas the basal surface area (BSA) makes up ~80% of the GSA.

2.2. Macroscopic Mixed-Flow Reactor Experiments

To obtain a bulk dissolution rate, experiments were performed in mixed-flow reactors (MFR). The experimental set up consists of a polyacryl reactor with a volume of 45 mL and a peristaltic pump. Typically MFR experiments were run for 200 h at pump rates between 0.5 (±0.005) and 1 (±0.01) ml/min. Dissolution experiments were carried out in solutions comprised of Milli-Q water (18.2 mΩ), HCl (ultrapure, Merck), and high purity $NaClO_4$ (99,9%, Merck) as background electrolyte. No additional additives or buffers were used. Samples of 50 mL were collected periodically in PTFA containers and immediately preserved for further analysis. The pH of each sample was measured with an accuracy of 0.04 pH units at the time it was sampled using a WTW inoLab 3 pH-meter equipped with a WTW Sentix 21 electrode.

The concentrations of Si and Fe were determined with a UV/VIS photometer using commercially available colorimetric methods (Merck product numbers 1.14764.0001, 1.14761.0001). Mg, Al and control measurements for Fe concentrations were performed using ICP-MS (Perkin Elmer Elan 5000). Within the experimental error of ~5% the Fe ICP-MS and colorimetric measurements were in good agreement.

During the MFR experiments, solution was pumped through the reactor at 0.5 to 1 mL/min. The solution entered and left the reaction vessel through 0.45 μm teflon filters (Millipore HVLP type). For each experiment 0.5g of chlorite powder were placed in the reactor. During the experiment the reactor was kept at 25±1°C by a thermostat. The chlorite suspension was continuously stirred by a suspended magnetic teflon stirring bar. Similar studies with biotite have shown, that the reaction history may alter the dissolution rate (Acker and Bricker, 1995). Therefore our dissolution experiments were conducted as single pH experiments starting with fresh chlorite samples.

To avoid affinity effects on the dissolution rate or the precipitation of secondary phases, all experiments were conducted far from equilibrium with respect to chlorite by adjusting the amount of chlorite and the pump rate (effluent concentrations of each element are presented in Table 3). The saturation index of the solution with respect to other

Table 3b. Saturation indices for selected phases calculated with the speciation program PHREEQC (Parkhurst & Appelo, 1999) for the experimental steady state concentrations of each element.

		Saturation index = log10 (ion activity product/solubility product)			
Phase	Chemical composition	pH 2	pH 3	pH 4	pH 5
Beidellite	$Mg_{0.165}Al_{2.33}Si_{3.67}O_{10}(OH)_2$	−29.11	−23.05	−18.47	−11.17
Boehmite	AlO(OH)	−8.07	−5.33	−2.73	0.21
Brucite	$Mg(OH)_2$	−18.40	−16.64	−15.02	−13.08
Chamosite	$Fe_2Al_2SiO_5(OH)_4$	−58.38	−48.22	−40.68	−32.13
Clinochlore	$Mg_5Al_2Si_3O_{10}(OH)_8$	−96.76	−82.98	−71.11	−55.44
$Fe(OH)_2$	$Fe(OH)_2$	−23.17	−20.75	−19.34	−18.02
$Fe(OH)_3$ (a)	$Fe(OH)_3$	−6.61	−4.18	−2.78	−1.46
Goethite	FeOOH	−1.50	0.93	2.33	3.65
Kaolinite	$Al_2Si_2O_5(OH)_4$	−19.83	−14.69	−10.43	−4.49
Nontronite	$Mg_{0.165}Fe_2Al_{0.33}Si_{3.67}H_2O_{12}$	−12.82	−7.39	−5.21	−1.14
SiO_2 (a)	SiO_2	−3.29	−3.46	−3.94	−3.90

phases which potentially precipitate (Table 3) was calculated for the respective steady state conditions with the speciation program PHREEQC (Parkhurst and Appelo, 1999). The speciation calculations were performed using the database from 'thermo.com.V8.R6.230' prepared by Jim Johnson at Lawrence Livermore National Laboratory.

Dissolution rates for mixed-flow reactor experiments can be calculated according to the following equation (Chou and Wollast, 1984; Knauss and Wolery, 1988; Knauss and Wolery, 1989; Nagy et al., 1991; Nagy and Lasaga, 1992):

$$\text{rate} = -\frac{F}{A \cdot m \cdot \nu_i} \cdot \Delta C_i \tag{3}$$

where Δc_i represents the concentration difference between the inlet and the outlet concentration of the ith element in solution, F for the fluid flow rate, ν_i represents the stoichiometric number of moles of the i^{th} element in one mole of chlorite, A is the specific surface area of the chlorite sample, m the mass of chlorite present in the reactor.

The total error of the rate is estimated to be around 15%, considering the uncertainties in the determination of A, Δc_i and the fluid flow rate. This value is in the range of the standard deviation of dissolution rates calculated from repetitive experiments at pH 2 and pH 4.

2.3. Microscopic Experiments

In contrast to earlier studies, where the sample was preetched for in-situ dissolution experiments (Rufe and Hochella Jr., 1999), we have used a sample which was preconditioned under steady state conditions. This enabled us to study the dissolution of a chlorite basal surface with a surface topography equilibrated to the conditions of the dissolution experiment. Microscopic dissolution experiments were performed on the chlorite CCa-2 sample from a 3 month steady state dissolution experiment performed at pH 2 and 25°C. The dissolution of this chlorite (001) surface was studied in-situ on a molecular scale using a Digital Instruments Nanoscope IIIa Multimode atomic force microscope (AFM) with a commercially available fluid cell. All images were obtained with the AFM operating in tapping mode (TM-AFM) using Si single crystal high aspect-ratio tips.

A suspension of chlorite (~0.15 g/L, grain size 10 to 63 μm) was mounted onto a sample holder which was coated by a thin layer of Tempfix® (Neubauer Chemicals, Germany. Technique described in detail by Bickmore et al., 1999). Tempfix® is a thermoplastic adhesive polymer that has similar properties as PE and is completely inert in the acid pH-range (Neubauer Chemikalien, personal communication). The chlorite particles were allowed to sediment from suspension. As a result of this sedimentation technique the chlorite grains were firmly attached with their basal (001) surface to the Tempfix®.

During the in-situ dissolution experiments, dissolution of the (001) surface proceeds via removal of material from molecular steps. AFM can be used to directly measure the step retreat rates. The step retreat rate was determined from a sequence of images using the WSxM (Nanotech electronica, Spain) and imagetool analysis (UTHSCSA, Texas) software. Dissolution rates were derived from a sequence of two images of dissolving chlorite as (Rufe and Hochella Jr., 1999):

$$\text{rate} = \frac{\Delta V / V_m}{SA(t)} \tag{4}$$

where ΔV is the volume of chlorite removed from respective feature on the chlorite surface, V_m is the molar volume of the chlorite (based on a complete formula unit), t is the time interval, and SA is the surface area determined as length x height of the steps. Dissolution rates were normalized to the edge surface area (ESA) of the $\{h k 0\}$ edges of the respective surface feature in the first image of each sequence.

Microscopic dissolution experiments were performed at pH 2 and 29 °C. The temperature of 29°C is due to minor warming up of the AFM fluid cell by the electronic devices of the AFM during the in-situ experiments. The original dissolution rates were recalculated to 25 °C assuming an dependency of the rates with temperature following the empirical Arrhenius equation:

$$\text{rate} = \text{A} \exp\left(\frac{-E_a}{RT}\right) \tag{5}$$

where A designates a preexponential factor, E_a refers to the activation energy, R is the gas constant and T is the temperature in K. For the dissolution of sheet silicates, depending on pH an activation energy of 45 to 88 kJ/mol has been reported (Nagy, 1995). For the recalculation of our rates to 25°C we have assumed an activation energy of 60 kJ/mol.

3. RESULTS AND DISCUSSION

3.1. Macroscopic Studies

3.1.1. Initial rate vs. steady state rate

The evolution of the dissolution rate with time (Fig. 1) for all our experiments shows the typical behaviour observed for mixed-flow experiments with sheet silicates (e.g., Malmström and Banwart, 1997; Metz and Ganor, 2001): (1) After an initial dissolution phase of ~50 h with a higher rate follows; (2) a steady state with a time independent rate.

The higher rates measured at the beginning of the experiments are due to dissolution of high energy surface sites, highly strained areas on large grains and ultrafine particles (Chou and Wollast, 1984; Knauss and Wolery, 1989; Wherli, 1989; Casey and Bunker, 1990). Within this study, steady state is defined to be reached, when the dissolution rate as a function of time remains constant within the experimental error. In general, steady state dissolution was reached during our experiments within the first 48 h with BET-surface area normalized rates

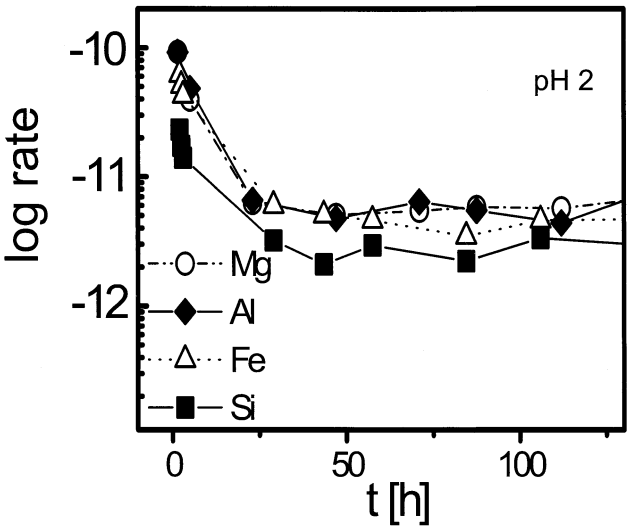

Fig. 1. Temporal evolution of the dissolution rate during a mixed-flow experiment with chlorite CCa-2 at pH 2 and 25°C with 0.1n $NaClO_4$ background electrolyte. All macroscopic dissolution rates are normalized to the chemical composition and to the BET-surface area of chlorite sample.

ranging in the order of 10^{-12} to 10^{-13} mol/m^{2}s (Fig. 2, Table 3).

The steady state rates as determined in this study are slightly higher than the chlorite dissolution rate calculated from multi mineral batch experiments by Salmon and Malmström (2001; Table 4) at pH 3.5. Lowson et al. (2002) obtained a very similar dissolution rate as in this study for pH 5, but slightly higher rates for lower pH values. This may be due to the experimental conditions. In contrast to our study, Lowson et al. (2002) used a potassium hydrogen phthalate buffer for the pH range 3 to 5

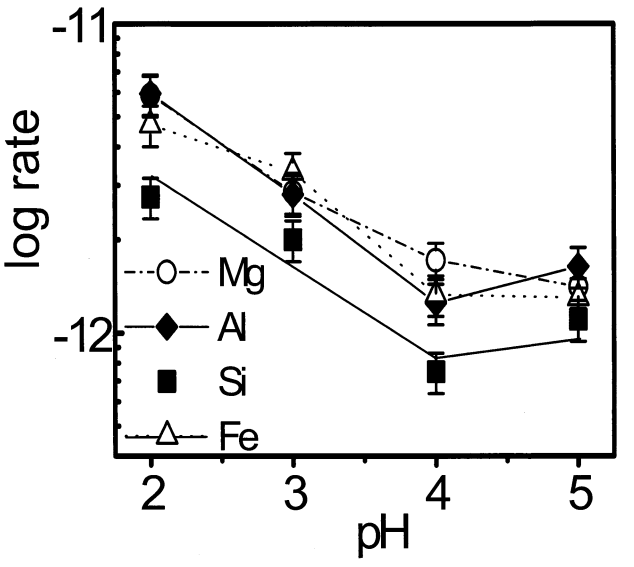

Fig. 2. Average steady-state dissolution rates of chlorite sample CCa-2 as a function of pH calculated from the release rate of the specific cation at 25°C with 0.1n $NaClO_4$ background electrolyte .

to maintain constant pH conditions during the MFR experiments. Furthermore, the differences between the dissolution rates generated in this study and in those of previous workers may be due to aqueous solution compositional effects of one or more of the constituent metals, which are also dependent on the experimental conditions such as pump rate and/or use of a buffer.

3.1.2. Stoichiometry of the dissolution reaction

In addition to the absolute dissolution rate, element release rates can be used to gather information about the stoichiometry of the dissolution reaction. For most sheet silicates congruent dissolution is reported for steady state conditions (Caroll and Walther, 1990; Nagy et al., 1991; Cama et al., 1994; Metz and Ganor, 2001). Incongruent dissolution is typical for the initial dissolution phase of many silicates (Caroll-Webb and Walther, 1988; Nagy, 1995; Oelkers, 2001a). Under steady state conditions incongruent dissolution of biotite was found to coincide with the formation of vermiculite (Malmström and Banwart, 1997). However, Malmström and Banwart (1997) hypothesized that the incongruent dissolution observed within the time frame of their experiments will eventually lead to a congruent dissolution. For a Mg-rich chlorite, May et al. (1995) report incongruent steady state dissolution at pH 3 to 5 and 25°C.

In our experiments, Si was released at a lower rate than the other cations (Al, Mg, Fe) from both chlorite samples, even when steady state was reached at pH 2. The Si release rates normalized to the chemical composition and specific surface area are only ~50 to 60% of the other cations' normalized release rates (Table 3). The normalized cation release rates follow the sequence Al > Mg > Fe > Si, which is similar to the relative content of each cation in the brucite-like layer. In both samples, almost 50% of the total Al is located in the brucite-like layer. Only 20% of the total Fe in sample MaIn and 33% of the total Fe in sample CCa-2 are located in the brucite-like layer. Based on the assumption, that all cations of the TOT-sheet are released at the same rate as Si, and taking into account the cation distribution presented above, the brucite-like layer dissolves ~2 to 2.5 times faster than the TOT sheet.

Our macroscopic experiments with chlorite CCa-2 indicate a similar preferential release of octahedrally coordinated cations for the pH range up to pH 4. For pH 3 and 4 (0.1mol/L $NaClO_4$), Si dissolution rates are ~60 to 70% of the other cations. For pH 5 no significant difference in the steady state rates of Si and the other cations was observed.

Long term experiments with CCa-2 have shown, that dissolution remains incongruent with respect to Si. Chemical analysis of Fe and Si of samples taken from a long term steady state dissolution experiment at pH 2, 25°C indicate incongruent dissolution even after 2000 h and a similar degree of non-stoichiometry as in the short term experiments. We hypothesize, that the brucite-like layer is leached from the grain edges inward

For the acid chlorite weathering a preferred dissolution of the brucite-like layer was also observed for Mg-chlorites (May et al., 1995). In fact, several studies (Table 4) indicate that chlorite dissolves incongruently under all pH conditions except for the near neutral pH-range (May et al., 1995; Malmström et al., 1996; Rochelle et al., 1996). For the basic pH range, a preferred

Table 4. Chlorite steady state dissolution rates as determined in earlier studies.

pH	Sample	Dissolution rate [10^{-12}mol/m^{2}s]				
		Si	Al	Mg	Fe	Reference
3.5	Chlorite (chemical composition not specified)	0.14	–	–	–	Salmon et al. 2001
5	Mg-clinochlore $(Mg_{9.8}Al_{1.8}Fe^{2+}_{0.2}Fe^{3+}_{0.2})[Si_{6.0}Al_{2.0}O_{20}](OH)_{16}$	0.3	–	–	–	May et al. 1995
8.2	Mg-chlorite $(Mg_{9.8}Al_{1.4}Fe^{2+}_{0.2}Fe^{3+}_{0.2})[Si_{7.0}Al_{1.0}O_{20}](OH)_{16}$	26	–	5.8	–	Malmström et al. 1996
7.7	Fe-chlorite (source clay) $(Mg_{5.36}Al_{2.62}Fe_{3.94})[Si_{5.56}Al_{2.46}O_{20}](OH)_{16}$	0.35	–	0.25	–	Rochelle et al. 1996
				0.50		
9.9	Fe-chlorite (source clay) $(Mg_{5.36}Al_{2.62}Fe_{3.94})[Si_{5.56}Al_{2.46}O_{20}](OH)_{16}$	1.00	–	0.50	–	Rochelle et al. 1996
12.5	Fe-chlorite (source clay) $(Mg_{5.36}Al_{2.62}Fe_{3.94})[Si_{5.56}Al_{2.46}O_{20}](OH)_{16}$	6	1.50	–	0.20	Rochelle et al. 1996

dissolution of the TOT sheet has been reported (Rochelle et al., 1996).

Experiments with and without 0.1mol/L $NaClO_4$ indicate only small effects of ionic strength (Table 3). The dissolution rate of CCa-2 at pH 2 is slightly lower in the presence of the background electrolyte, but remains incongruent with a rate derived from Si measurements that is only 50% of the rate calculated for the other cations.

3.1.3. Deviation from equilibrium

The saturation index for relevant phases that might precipitate during the mixed-flow reactor experiments was calculated for the experimental conditions using the speciation program PHREEQC (Parkhurst and Appelo, 1999). Our calculations indicate (Table 3), that some experiments were supersaturated with respect to several iron phases, which are not likely to precipitate within the time scale of our experiments. The amorphous Fe-phases, which may precipitate very quickly when supersaturated, were undersaturated. Although the solubility of these amorphous Fe-phases is not well defined, calculations with the PHREEQC database (log K_{so} for $Fe(OH)_3$ (am) = -12.56) indicate that all experiments were undersaturated with respect to amorphous iron phases.

Solubility data for hydrous aluminium silicate phases (HAS) are not available within the databases used in this study. Therefore we cannot definitely exclude the fact, that secondary phases may have formed. Even if Hematite and Goethite or HAS were formed, these particles would very likely be smaller than the filter pore size of 450 nm (Schwertmann and Cornell, 2000). Therefore these particles may have been small enough to leave the mixed-flow reactor through the filter.

3.1.4. Effect of pH

The dependency of surface reaction controlled dissolution rates far from equilibrium as a function of pH is often described by an empirical rate law (Blum and Lasaga, 1988; Stumm and Wollast, 1990)

$$R = k_H [H^+]^m + k_0 + k_{OH}[H^+]^n \quad (6)$$

where k_H, k_0 and k_{OH} are the rate constants and n and m the reaction orders. The reaction order m as determined by linear regression from our experimental data (0.1 mol/L $NaClO_4$ background electrolyte, HCl) in the pH range between 2 and 4 is $\sim 0.29 \pm 0.05$ for all cations (Fig. 2). This is considerably lower than what has been reported for the acid dissolution of Mg-rich chlorites (m = 0.5; May et al., 1995) in H_2SO_4 and Fe chlorites (m = 0.6 Lowson et al., 2002), which were dissolved in buffered potassium hydrogen phthalate/HCl solutions. Therefore, the presence of an organic buffer may influence the dependency of the dissolution rate as a function of pH. Also, the differences in the hydrogen reaction orders may be an artefact due to solution compositional effects, which may be generated by variation of experimental conditions such as the pump rate and/or the use of a buffer.

3.2. Microscopic Studies

3.2.1. Steady state particle morphology and topography

To characterize the morphology and topography of a chlorite sample CCa-2 after steady state dissolution, macroscopic long term experiments were performed at pH 2 and 25°C using the grain size 10 to 63μm. We expect the most substantial effects on particle morphology at pH 2, because dissolution was fastest under these conditions within the pH-range of the macroscopic experiments. The chlorite sample was examined with field-emission scanning electron microscopy (FE-SEM) and TM-AFM before the dissolution experiment and after 3 months of steady state dissolution.

The fresh chlorite sample was characterized by grains with an irregular shape and smooth basal surfaces (Fig. 3a). The edges of these particles were broken and stepped. This morphology may be due to the heating and cooling preparation technique, where chlorite aggregates were mechanically separated into small particles. Within the basal surfaces we commonly observed cracks (Fig. 3a, indicated by arrows). TM-AFM observations indicate that the basal surfaces were very smooth, with steps limited to the cracks and to the edges of the particles.

Compared to the initial chlorite CCa-2 morphology, only minor changes were observed after the 3 month steady state dissolution experiments. However, within the basal surfaces of the chlorite sample subjected to the dissolution experiment, we find channel like features, which may originate from the cracks

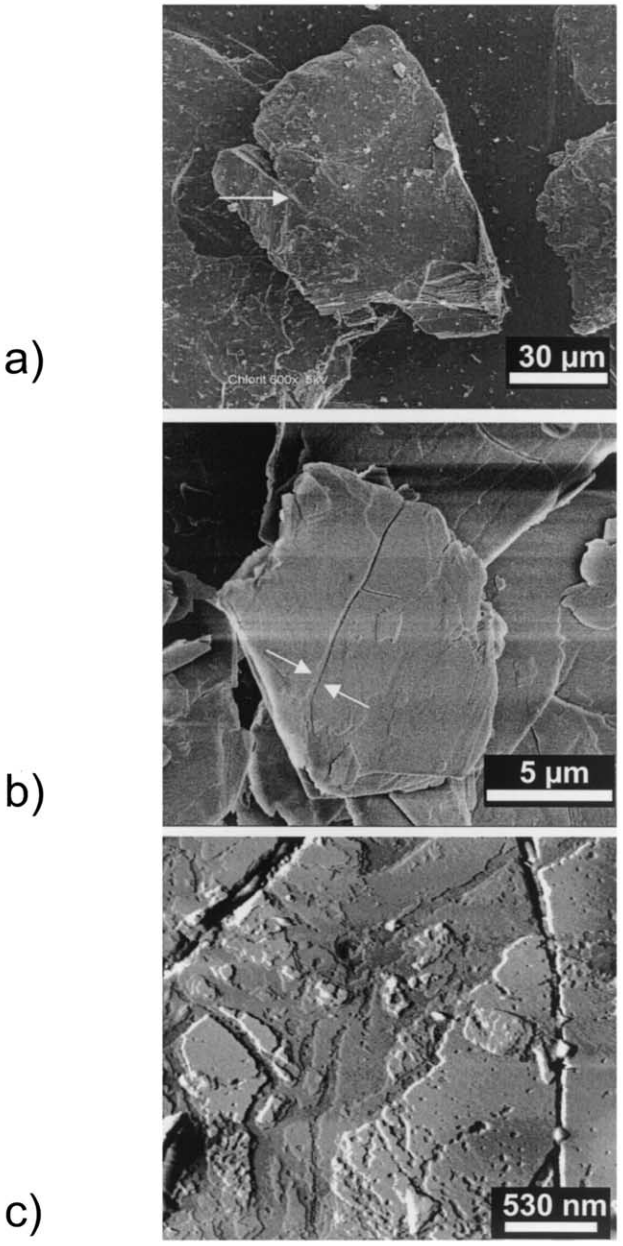

Fig. 3. a) FE-SEM image (carbon coating, 3kV) of a chlorite CCa-2 particle before the dissolution experiment. The arrow indicates a crack in the basal surface; b) FE-SEM image of a CCa-2 chlorite particle weathered at pH 2, 25°C. For this experiment the grain fraction 10 to 63 μm was used. The arrows in indicate the formation of dissolution channels. c) Tapping mode AFM image of a chlorite (001) surface of one of the particles weathered at pH 2, 25 °C at the beginning of an in-situ AFM dissolution experiment at pH 2.

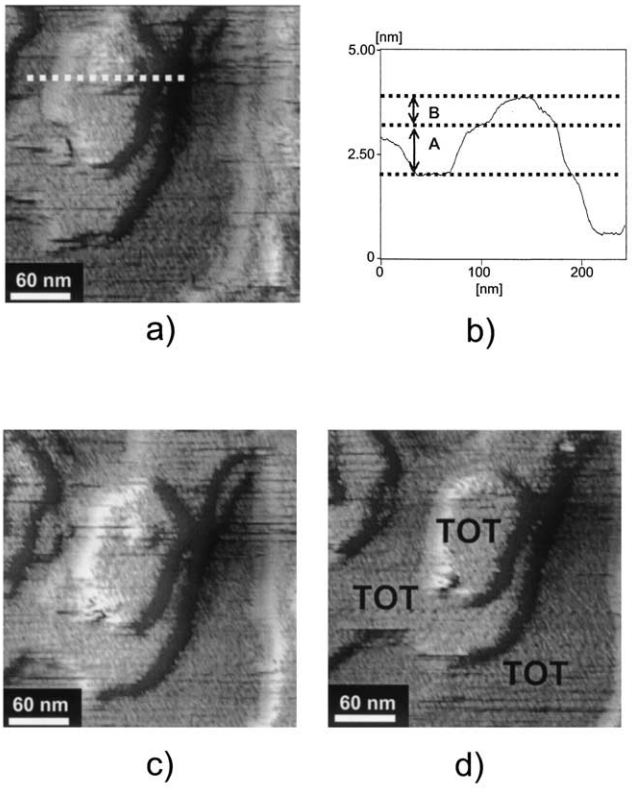

Fig. 4. In-situ tapping mode AFM dissolution sequence at pH 2 and 29±1°C taken on the surface shown in Figure 3c. The profile in Figure 4b was taken along the dotted line in Figure 4a. The height difference A corresponds to one TOT layer, whereas the height difference B corresponds to one brucite-like layer. Figure 4c taken 250 and Figure 4d taken 830 s after Figure 4a.

of the initial sample. These features were also observed in early studies during chlorite dissolution in the acid pH-range at much higher acidity and temperature (2n HCl, 97°C), where they were described as *solution channels* (Ross, 1969). Based on his observations, Ross (1969) suggested that dissolution of chlorite was not just simply a process happening at the grain edges, but occurs primarily at cracks and structural defects.

On the molecular scale, TM-AFM observations of the CCa-2 chlorite sample basal surface after the dissolution experiment support Ross' hypothesis. In contrast to the original sample, isolated etch pits were observed, which are typically only a few nanometers in depth and therefore not visible with SEM (Fig. 3c, 4). The maximum height difference between the highest and the lowest point on the weathered chlorite surface within a scanning area of 2.6 × 2.6μm is typically ~7 nm. In addition, the entire surface is covered with molecular steps of different step heights, which mainly originate at the *solution channels*. After dissolution at pH 2 under steady state conditions, repetitive TM-AFM measurements of step heights and lengths indicate that the molecular steps contribute to ~2% of the basal surfaces.

Steps with a height difference of 3, 4, 7, 10 and 14Å were observed. A height difference of 14Å corresponds to the (001) lattice plane distance of one chlorite unit cell. Steps with a height difference of 14 Å or a multiple of 14Å are by far the most frequently observed steps. Repetitive TM-AFM measurements of step heights and lengths indicate, that ~90% of the molecular step edge surface area is associated with the 14Å steps. The 10Å height difference is very similar to the lattice plane distance of a TOT-sheet parallel to the chlorite (001) surface, a 7Å step height to the lattice plane distance of one tetrahedral sheet and one octahedral sheet; the 4Å step height is similar to the lattice plane difference of one brucite like layer,

Table 5. Chlorite CCa-2 dissolution rates as determined with AFM and macroscopic experiments for pH 2. The microscopic rates were corrected to 25 °C using the Arrhenius approach and an activation energy of 60 kJ/mol.

Macroscopic Dissolution Rates [mol/m^{2}s]			
	BET normalized	GSA-normalized	RSA-normalized
Si-Rate (mol/m^{2}s)	$3{,}21 \cdot 10^{-12}$	$4{,}17 \cdot 10^{-11}$	$2{,}61 \cdot 10^{-9}$
Mg-Rate (mol/m^{2}s)	$5{,}60 \cdot 10^{-12}$	$7{,}28 \cdot 10^{-11}$	$4{,}55 \cdot 10^{-9}$
step retreat rates [nm/min]		RSA-normalized microscopic Rates [mol/m^{2}s]	
	at 29 °C	at 29 °C	corrected to 25 °C
14 Å steps	0.05–0.3	$2.5\ (\pm 1.3) \cdot 10^{-9}$	$2.5 \cdot 10^{-9}$
10 Å steps	0.4–1.2	$4.3\ (\pm 2.1) \cdot 10^{-8}$	$3.1 \cdot 10^{-8}$
4 Å steps	1.8–3	$2.9\ (\pm 1.5) \cdot 10^{-7}$	$2.1 \cdot 10^{-7}$
7 Å steps	0.4–1.2		
3 Å steps	0.4–1.2		

BET = BET surface area; GSA = geometric surface area; RSA = reactive surface area.

whereas the 3Å match the lattice plane distance of just one tetrahedral sheet.

Although steps with various height differences were observed with TM-AFM, after 3 month steady state dissolution under acidic conditions, most of the chlorite (001) surface is terminated by terraces which are limited by steps with a height difference of 10Å, i.e., almost the complete chlorite basal surface is terminated by Si and Al tetrahedrons.

3.2.2. Dissolution kinetics on a molecular scale

The dissolution process was monitored in real time in microscopic in-situ dissolution experiments, which were performed on the (001) surface of the chlorite CCa-2 sample described in section 3.2.1 at pH 2 and 29°C. Under these conditions the dissolution of the chlorite basal surface primarily occurs via the retreat of molecular steps. The molecular step edges are the most reactive surface area during the dissolution process. The surface area of the molecular steps represents ~2% of the total surface area of the chlorite basal surface. The step density remains constant during our in-situ AFM experiments at pH 2.

During the pH 2 in-situ dissolution experiment we observed different retreat velocities for molecular steps, depending on the step height. The 14 Å steps retreat at velocities of 0.05 to 0.3 nm/min, whereas the 10 Å TOT steps of chlorite retreat with velocities of ~0.4 to 1.2 nm/min (hectorite: 0.15 to 1.2 nm/min, Bosbach et al., 2000; phlogopite 0.02 nm/min; Rufe and Hochella Jr., 1999). The 7 Å steps retreat at similar velocities as the TOT steps. The 4 Å brucite-like layer dissolves at much higher rates, with step velocities of 1.8 to 3 nm/min (Fig. 4).

A dissolution rate was calculated from the step retreat velocities (Table 5). For the 14 Å steps we calculated a dissolution rate of $2.5\ (\pm 1.3) \times 10^{-9}$ mol/m^{2}s (recalculated to 25°C). This dissolution rate is in the range of the ESA- normalized dissolution rate of phlogopite, 3.7×10^{-10} mol/m^{2}s (Rufe and Hochella Jr., 1999) and hectorite, 7.3×10^{-9} mol/m^{2}s (Bosbach et al., 2000). However, the ESA-normalized dissolution rates of phlogopite and hectorite were calculated from the dissolution of 10 Å TOT steps. An ESA-normalized dissolution rate (recalculated to 25°C assuming an activation energy of 60 kJ/mol) of 3.1×10^{-8} mol/m^{2}s was calculated for the dissolution of 10 Å TOT steps, which amount to less than 10% of the all steps on the (001) surface. An ESA-normalized dissolution rate of the brucite-like layer was calculated to be 2.1×10^{-7}mol/m^{2}s (recalculated to 25°C, using the activation energy of 60 kJ/mol as determined by Jordan and Rammensee, 1996 for the mineral brucite). This rate is one order of magnitude higher than the rate determined for the TOT-sheet. Compared to the observations of studies on the dissolution of single crystals of the mineral brucite at pH 2.7 and 21°C (Jordan and Rammensee, 1996) the step velocities and the dissolution rate of the brucite-like layer of chlorite at pH 2 is about two orders of magnitude slower. This difference may be due to the substitution of Al and Fe for Mg in the brucite-like interlayer may also affect its dissolution rate compared to pure $Mg(OH)_2$. The mineral gibbsite ($Al(OH)_3$) dissolves several orders of magnitude slower than the mineral brucite (Nagy, 1995).

3.2.3. Formation of etch pits on the chlorite (001) surface

The formation of etch pits was observed within flat terraces on the (001) chlorite surface during the in-situ experiments at pH 2. Etch pits were observed through both, the TOT layer and the brucite like layer. However, no etch pits were observed, which run continuously through more than one TOT or brucite like layer.

The formation of etch pits within the TOT sheet (square in Fig. 5a and 5b) on the (001) chlorite surface is a process that involves several individual steps. At first a pit of ~7 Å depth is formed. Apparently, one tetrahedral sheet (3 Å) and one octahedral sheet (4 Å) are dissolved at the same time. However, it is also possible that within the time frame of an AFM scan of ~2.5 min/image, first a tetrahedral sheet and then the octahedral sheet dissolves. About 30 min after the opening of the etch pit a new etch pit with a depth of 3 Å, corresponding to one tetrahedral sheet, opens within the first etch pit (arrow in Fig. 5a). Apparently, single tetrahedral sheets are temporarily stable and more stable than the octahedral sheet. The 3 Å steps retreat with velocities of ~2 to 3 nm/min until they close up with the border of the 7 Å step etch pit (Fig. 5b).

Etch pits within the brucite-like layer can be observed when the brucite-like layer is not covered by a TOT sheet. This

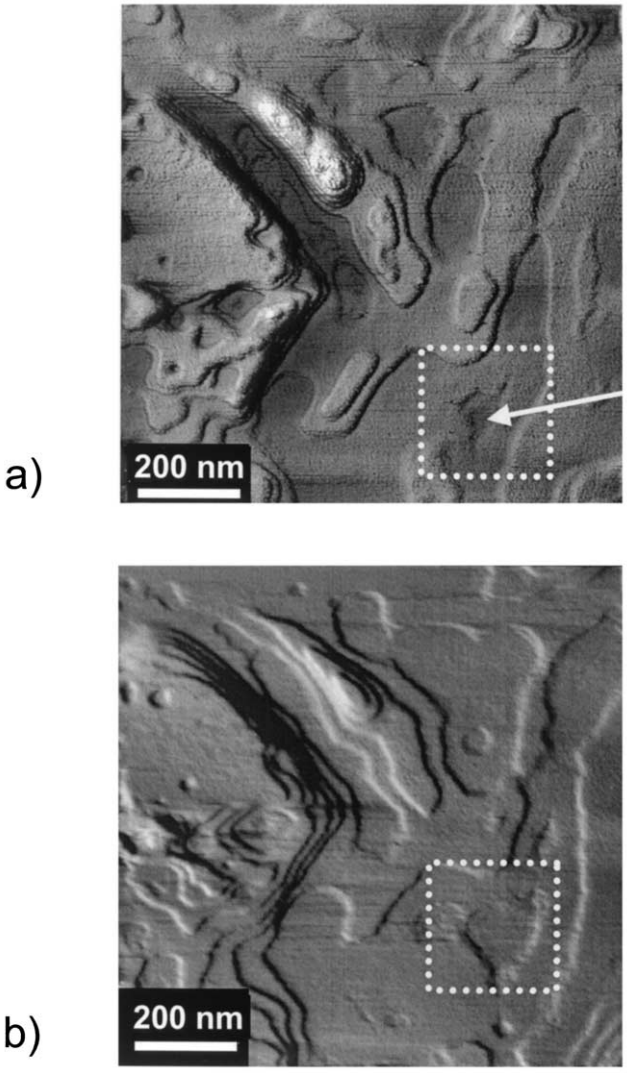

Fig. 5. a) In-situ tapping mode AFM dissolution sequence at pH 2 and 29±1°C taken on the surface shown in Figure 3c showing the opening of an etch pit within a TOT layer. b) The same surface 1200s after Figure 5a. The etch pit marked by the square is now 10 Angstroms in depth, corresponding to one TOT sheet.

observation indicates, that the brucite-like layer also is temporarily stable to acid attack. As soon as etch pits are formed, the 4 Å steps retreat rapidly at step velocities of 1.8 to 3 nm/min.

3.3. The Reactive Surface Area

The reaction rate of surface controlled mineral dissolution is a function of the number of reactive sites at the mineral/water interface, e.g., aluminol groups (Al-O-H) or silanol groups (Si-O-H). To be able to be able to extrapolate to the field scale, macroscopic dissolution rates are commonly normalized to some surface area which is assumed to be proportional to the number of reactive sites: the reactive surface area. Thus, the reactive surface area is used to link the microscopic dissolution mechanisms and the bulk dissolution rate.

Depending on the mineral, different models for a reactive surface area have been proposed: (1) the reactive surface area is equal to the total surface area (e.g., BET surface area); (2) the reactive surface area is limited to certain crystal faces; or (3) the reactive surface area is dominated by surface defects such as compositional inhomogenities (Nagy, 1995).The reactive surface area of minerals during dissolution is commonly assumed to be the BET surface area or to be proportional to the BET surface area (e.g., Ganor et al., 1999). However, in some studies on the dissolution of sheet silicates almost constant element release rates were measured, although the BET surface area changed significantly (up to 90%) during the experiment (Cama et al., 2000).

For phyllosilicates, such as hectorite, nontronite and phlogopite, the edge surfaces of the respective mineral were identified as the only reactive surfaces, whereas the basal surfaces were nearly inert (Rufe and Hochella Jr., 1999; Bosbach et al., 2000; Bickmore et al., 2001). AFM studies on nontronite and hectorite have also shown (Bosbach et al., 2000; Bickmore et al., 2001), that the reactive surface area is not a constant, but changes as dissolution proceeds. Therefore for these minerals the reactive surface area is not proportional to the BET or geometric surface area.

For the chlorite used in this study, we have proposed two different, independent mechanisms of dissolution: dissolution at defects at the basal surfaces and dissolution of the brucite layer from the grain edges inward. For the dissolution of the brucite like layer, it is difficult to determine a reactive surface area, as this process very likely involves diffusion within the chlorite structure.

On the chlorite (001) basal surfaces, molecular steps which originate at structural defects, were identified as the most reactive sites during dissolution. These defects are usually only expressed through a single TOT or brucite like layer and it is therefore very unlikely to find defects which allow the simultaneous dissolution of several layers. Earlier studies on muscovite suggested, that compositional impurities might control this kind of pit nucleation with very shallow depths (Johnsson et al., 1992). The defect controlled dissolution mechanism favours dissolution of molecular steps compared to dissolution of macro steps on the basal surfaces. If fast dissolution were initiated at a single layer in a macro step, it would soon have to slow down, because the reactants and products would have to diffuse between the layers above and below the fast dissolving one. Therefore, the reactivity of (hk0) molecular steps is much higher compared to the reactivity of (hk0) crystal faces.

The reactive surface area, i.e., the step edges' surface area, was determined from their height and length and related to the corresponding area of the basal surface. During in-situ dissolution experiments at pH 2 this surface area remains constant. This indicates a constant step density which might be a function of pH. For pH 2, a ratio reactive surface area/basal surface area of 0.02 was determined from repetitive experiments. For the macroscopic chlorite crystals we calculate a reactive surface area of $\sim 2\times10^{-3}$ m^2/g for the defect controlled dissolution mechanism, considering that the basal surfaces make up ~80% of the GSA of 0.12 m^2/g.

Normalizing the macroscopic dissolution rate to this reactive surface area, from the steady state Si release rate (pH 2, 25°C) we calculate a dissolution rate of 2.61×10^{-9} mol/m^2s. This corresponds well with the microscopic ESA normalized disso-

lution rate of 2.5 (± 1.3)$\times 10^{-9}$ mol/m^{2}s determined for the 14 Å molecular steps.

4. CONCLUSIONS

The dissolution of chlorite with intermediate Fe content was examined using a combined microscopic and macroscopic experimental approach. Our results indicate that two mechanisms seem to control chlorite dissolution at low pH: (1) defect controlled dissolution of molecular steps on the basal surfaces; and (2) transformation of parts of the chlorite structure into interstratified vermiculite/smectite.

In contrast to studies on nontronite and hectorite dissolution (Bosbach et al., 2000; Bickmore et al., 2001), in-situ microscopic observation indicate that surface defects such as cracks or compositional inhomogenities control the dissolution of the chlorite basal surfaces. The formation of nanoscale etch pits within flat terraces terminated by the TOT sheet was observed in-situ. The defects at which these etch pits originate are only expressed through single TOT or brucite like layers, favoring a layer by layer dissolution of molecular steps compared to dissolution at macro steps or the chlorite edge surfaces. Molecular steps which originate at these surface defects are the most reactive surface sites during acid dissolution. The dissolution 14 Å steps, which retreat at velocities of 0.05 to 0.3 nm/min, control the dissolution of the basal surface.

BET surface area normalized dissolution rates were determined from macroscopic steady state experiments in the pH range 2 to 5. The reaction order of the dissolution reaction with respect to protons was determined to be ~0.29. The macroscopic dissolution and the microscopic dissolution rate can be linked via normalization to the reactive surface area. The reactive surface normalized dissolution rates from the macroscopic (Si release rate) and microscopic approach are in good agreement (Table 5). A reactive surface area of 2.4×10^{-3} m^2/g was determined for the dissolution of chlorite at pH 2 compared to a BET surface area of 1.6 m^2/g.

Within the scope of our macroscopic experiments, for pH 2 to 4 a non-stoichiometric steady state dissolution with a preferential release of octahedrally coordinated cations was observed. Because dissolution on the basal surfaces is stoichiometric, we hypothesize that incongruent dissolution is due to selective leaching of Mg, Al and Fe from the brucite like layer from the grain edges inward. Studies on the dissolution of mulioxide silicate minerals (Oelkers, 2001b) suggest that the rate of Mg for H or Al for H exchange reactions is orders of magnitude faster than the breaking of Si-O bonds, which very likely involves H_2O adsorption rather than an Si for H exchange reaction. In the long run, this process may lead to the transformation into regularly and irregularly interstratified vermiculite/smectite, and because of increasing diffusion path length, to congruent dissolution. This observation is consistent with earlier studies on chlorite dissolution/weathering which indicate a transformation of chlorite into interstratified chlorite/vermiculite or chlorite/smectite (Adams and Kassim, 1983; May et al., 1995; Banfield and Murakami, 1998).

Acknowledgments—The authors would like to acknowledge the help of: V. Rapelius (Universität Münster), H. Heying (Universität Münster), C. Schmitt-Riegraf (Universität Münster) H. Geckeis (Karlsruhe), F. Geyer (Karlsruhe), H. Pieper (Karlsruhe), K. Henkel (Dresden) and U.Schaefer (Dresden). This study has received financial support from the Deutsche Forschungsgemeinschaft, (DFG Project BO 1455/1 to 2 and BE 2234/4 to 2).

The authors would also like to acknowledge the review by Barry Bickmore, Maria Malmström, one anonymous reviewer and the associate editor Eric Oelkers.

Associate editor: E. H. Oelkers

REFERENCES

Acker J. G. and Bricker O. P. (1995) The Influence of pH on Biotite Dissolution and Alteration Kinetics at low-temperature. *Geochim. Cosmochim. Acta* **56**(8), 3073–3082.

Adams W. A. (1976) Experimental evidence on the origin of vermiculite in soils of lower Palaeozoic sediments. *Soil Sci. Soc. Am. J.* **40,** 793–796.

Adams W. A. and Kassim J. K. (1983) The origin of vermiculite in soils developed from lower Palaeozoic sedimentary rocks in Mid-Wales. *Soil Sci. Soc. Am. J.* **47,** 316–320.

Arnold T., Zorn T., Zanker H., Bernhard G., and Nitsche H. (2001) Sorption behavior of U(VI) on phyllite: experiments and modeling. *J. Cont. Hydrol.* **47**(2–4), 219–231.

Bain D. C. (1977) Weathering of chlorite minerals in some Scottish soils. *Soil Sci. Soc. Am. J.* **28,** 144–164.

Banfield J. F. and Murakami T. (1998) Atomic-resolution transmission electron microscope evidence for the mechanism by which chlorite weathers to 1:1 semi-regular chlorite-vermiculite. *Am. Mineral.* **83**(3–4), 348–357.

Barnhisel R. I. and Bertsch P. M. (1989) Chlorites and Hydroxy-Interlayered Vermiculite and Smectite. In *Minerals in Soil Environments*. Soil Science Society of America.

Bickmore B. R., Bosbach D., Hochella M. F., Charlet L., and Rufe E. (2001) In situ atomic force microscopy study of hectorite and nontronite dissolution: Implications for phyllosilicate edge surface structures and dissolution mechanisms. *Am. Mineral.* **86**(4), 411–423.

Bickmore B. R., Hochella M. F., Bosbach D., and Charlet L. (1999) Methods for performing atomic force microscopy imaging of clay minerals in aqueous solutions. *Clays Clay Min.* **47**(5), 573–581.

Blum A. E. and Lasaga A. C. (1988) Role of surface speciation in the low-temperature dissolution of minerals. *Nature* **331,** 431–433.

Bosbach D., Charlet L., Bickmore B., and Hochella M. F. (2000) The dissolution of hectorite: In-situ, real-time observations using atomic force microscopy. *American Mineral.* **85**(9), 1209–1216.

Brantley S. and Chen Y. (1995) Chemical Weathering Rates Of Pyroxenes and Amphiboles. In *Reviews in Mineralogy* (ed White A. F. and Brantley S. L.) **Vol. 31** pp. 119–172. Min. Soc. Am.

Brindley G. W. and Brown G. (1984) Crystal Structures of Clay Minerals and their X-Ray Identification. Mineralogical Society.

Brunauer S., Emmet P. H., and Teller E. (1938) Adsorption of gas in multimolecular layers. *J. Am. Chem. Soc.* **60,** 309–319.

Cama J., Ayora C., and Lasaga A. C. (1999) The deviation-from-equilibrium effect on dissolution rate and on apparent variations in activation energy. *Geochim. Cosmochim. Acta* **63**(17), 2481–2486.

Cama J., Ganor J., Ayora C., and Lasaga C. A. (2000) Smectite dissolution kinetics at 80 degrees C and pH 8.8. *Geochim. Cosmochim. Acta* **64**(15), 2701–2717.

Cama J., Ganor J., and Lasaga A. C. (1994) The kinetics of smectite dissolution. *Min. Mag.* **58**(A), 140–141.

Caroll S. A. and Walther J. V. (1990) Kaolinite dissolution at 25°, 60° and 80°C. *Am J Sci.* **290,** 797–810.

Caroll-Webb S. and Walther J. (1988) A surface complex reaction model for the pH dependence of corundum and kaolinite dissolution rates. *Geochim. Cosmochim. Acta* **52,** 2609–2623.

Casey W. H. and Bunker B. (1990) Leaching of mineral and glass surfaces during dissolution. In *Mineral-Water Interface Geochemistry* (ed. M. F. Hochella Jr. and A. F. White) **Vol. 23**, pp. 397–426. Min. Soc. America.

Chou L. and Wollast R. (1984) Study of the weathering of albite at room temperature and pressure in a fluidized bed reactor. *Geochim. Cosmochim. Acta* **48,** 2205–2217.

Coffman C. B. and Fanning D. S. (1975) Maryland soils developed in residuum from chlorite metabasalt having high amounts of vermiculite in sand and silt fractions. *Soil Sci. Soc. Am. Proc.* **39,** 723–732.

Ganor J., Mogollon J. L., and Lasaga A. C. (1995) The Effect of pH on Kaolinite Dissolution Rates and on Activation-Energy. *Geochim. Cosmochim. Acta* **59**(6), 1037–1052.

Ganor J., Mogollon J. L., and Lasaga A. C. (1999) Kinetics of gibbsite dissolution under low ionic strength conditions. *Geochim. Cosmochim. Acta* **63**(11–12), 1635–1651.

Helgeson H., Murphy W., and Aagard P. (1984) Thermodynamic and kinetic constraints on reaction rates among minerals and aquaeous solutions. II. Rate constants, effective surface area, and the hydrolysis of feldspar. *Geochim. Cosmochim. Acta* **48,** 2405–2432.

Herbillon A. J. and Makumbi M. N. (1975) Weathering of chlorite in a soil derived from a chlritoischist under humid tropical conditions. *Geoderma* **13,** 89–104.

Herrmann G. A. (1975) *Praktikum der Gesteinsanalyse.* Springer.

Hochella M. F., Moore J. N., Golla U., and Putnis A. (1999) A TEM study of samples from acid mine drainage systems: Metal- mineral association with implications for transport. *Geochim. Cosmochim. Acta* **63**(19–20), 3395–3406.

Johnsson P., Hochella Jr. M. F., Parks G., Blum A. E. and Sposito G. (1992) Direct observation of muscovite basal-plane dissolution and secondary phase formation: An XPS,LEED and SFM study. In *Water Rock Interactions* (ed. Y. Kharaka and A. Maes), pp. 159–162. AA Balkema.

Jordan G. and Rammensee W. (1996) Dissolution rates and activation energy for dissolution of brucite (001): A new method based on the microtopography of crystal surfaces. *Geochim. Cosmochim. Acta* **60**(24), 5055–5062.

Joswig W., Fuess H., Rothbauer R., Takeuchi Y., and Mason S. (1980) A neutron diffraction studey of a one-layer triclinic chlorite (pennite). *Am. Mineral.* **65,** 349–352.

Knauss K. G. and Wolery T. J. (1988) The dissolution kinetics of quarz as function of pH and time at 70°. *Geochim. Cosmochim. Acta* **53,** 43–53.

Knauss K. G. and Wolery T. J. (1989) Muscovite dissolution kinetics as a function of pH and time at 70°C. *Geochim. Cosmochim. Acta* **53,** 1493–1501.

Krawczyk-Bärsch E., Arnold T., Hüttig G., Zänker H., Brandt F., Bosbach D., and Bernhard G. (2001). The effect of secondary iron mineral and colloid formation on uranium sorption during the dissolution of chlorite. In Eleventh Annual V. M. Goldschmidt Conference, Abstract Nr. 3161. LPI Contribution No. 1088, Lunar and Planetary Institute, Houston (CD-ROM).

Lougear A., Grodzicki M., Bertoldi C., Trautwein A. X., Steiner K., and Amthauer G. (2000) Mössbauer and molecular orbital study of chlorites. *Phys. Chem. Min.* **27**(4), 258–269.

Lowson R., Comarmond M., Rajaratnam G., and Brown P. (2002). Personal communication.

Malmström M. and Banwart S. (1997) Biotite dissolution at 25°C: The pH dependence of dissolution rate and stoichiometry. *Geochim. Cosmochim. Acta* **61**(14), 2779–2799.

Malmström M., Banwart S., Lewenhagen J., Duro L., and Bruno J. (1996) The dissolution of biotite and chlorite at 25°C in the near-neutral pH region. *J. Contam. Hydrol.* **21**(1–4), 201–213.

May H. M., Acker J. G., Smyth J. R., Bricker O. P., and Dyar M. D. (1995) Aqueous dissolution of Low-Iron Chlorite in dilute acid solutions at 25°C. 32nd Ann. Meeting Clay Minerals Society.

Metz V. and Ganor J. (2001) Stirring effect on kaolinite dissolution rate. *Geochim. Cosmochim. Acta* **65**(20), 3475–3490.

Moore D. M. and Reynolds R. C. (1997) X-Ray Diffraction and the Identification and Analysis of Clay Minerals. Oxford University Press.

Nagy K. L. (1996) Dissolution and precipitation kinetics of sheet silicates. In *Rev. Mineral* (ed. A. F. White and S. L. Brantley) **Vol. 31**, pp. 173–233. Mineralogical Society of America.

Nagy K. L., Blum A. E., and Lasaga A. C. (1991) Dissolution and precipation kinetics of kaolinite at 80°C and pH 3: The dependence on solution saturation state. *Am. J. Sci.* **291,** 649–686.

Nagy K. L. and Lasaga A. C. (1992) Dissolution and precipitation kinetics of gibbsite at 80°C and pH 3: The dependence on solution saturation state. *Geochim. Cosmochim. Acta* **56,** 3093–3111.

Oelkers E. H. (2001a) An experimental study of forsterite dissolution rates as a function of temperature and aqueous Mg and Si concentrations. *Chem. Geol.* **175**(3–4), 485–494.

Oelkers E. H. (2001b) General kinetic description of multioxide silicate mineral and glass dissolution. *Geochim. Cosmochim. Acta* 65(21), 3703–3719.

Parkhurst D. and Appelo C. (1999) PHREEQC for Windows. A hydrochmical transport model. Graphical user interface by V.E.A. Post.

Rochelle C. A., Bateman K., MacGregor R., Pearce J. M., Savage D., and Wetton P. D. (1996) Experimental determination of chlorite dissolution rates. Materials Research Society Symposium.

Ross G. J. (1969) Acid dissolution of chlorites: Release of Magnesium, Iron and Aluminum and mode of acid attack. *Clays Clay Mineral.* **17,** 347–354.

Rufe E. and Hochella Jr. M. F. (1999) Quantitative Assessment of Reactive Surface Area of Phlogopite During Acid Dissolution. *Science* **285(5429),** 874–876.

Rule A. C. and Bailey S. W. (1987) Refinement of the crystal structure of a monoclinic ferroan clinochlore. *Clays Clay Mineral.* **35**(2), 129–138.

Salmon S. U., and Malmström M. E. (2001) Mineral weathering Rates in Mill Tailings From Kristinenberg, Northern Sweden. In *Eleventh Ann. V.M. Goldschmidt Conference, Abstract # 3375.* LPI Contribution No. 1088, Lunar and Planetary Institute, Houston (CD-ROM).

Schwertmann U. and Cornell R. M. (2000) Iron. Oxides in the Laboratory. Second Edition. Wiley-VCH Verlag.

Steinfink H. (1958a) The crystal structure of chlorite. I. A monoclinic polymorph. *Acta Crystall.* **11,** 191–195.

Steinfink H. (1958b) The crystal structure of chlorite. II. A triclinic polymorph. *Acta Crystall.* **11,** 195–198.

Steinfink H. (1961) Accuracy in structure analysis of layer silicates: Some further comments on the structure of prochlorite. *Acta Crystall.* **14,** 198–199.

Stumm W. and Wollast R. (1990) Coordination chemistry of weathering: Kinetics of the surface controlled dissolution of oxide minerals. *Rev. Geophys.* **28,** 53–69.

Turpault M. P. and Trotignon L. (1994) The dissolution of biotite single crystals in dilute HNO3 at 24°C: Evidence of an anisotropic corrosion process of micas in acidic solutions. *Geochim. Cosmochim. Acta* **58**(13), 2761–2775.

Wherli B. (1989) Monte Carlo simulations of surface morphologies during mineral dissolution. *J. Coll. Interface Sci.* **132,** 230–242.

White A. F. and Brantley S. L. (1995) Chemical Weathering Rates of Silicate Minerals: An Overview In *Rev. Mineral* (ed. A. F. White and S. L. Brantley) **Vol. 31,** pp. 1–21. Mineralogical Society of America.